

Supplementary Information

Hydrothermal synthesis and structure of organically templated layered neptunyl(VI) phosphate ($\text{NpO}_2)_3(\text{PO}_4)_2(\text{Terpy})$

Lei Zhang,^{*a,b,c} Yu Wang,^{b,d} Mengyu Xu,^e Alex M. Kokot,^a Jie Qiu,^{a,f} and Peter C. Burns^{a,e}

^a Department of Civil and Environmental Engineering and Earth Sciences, University of Notre Dame, Notre Dame, IN 46556, USA.

^b Zhejiang Key Laboratory of Data-Driven High-Safety Energy Materials and Applications, Ningbo Key Laboratory of Special Energy Materials and Chemistry, Ningbo Institute of Materials Technology and Engineering, Chinese Academy of Sciences, Ningbo 315201, China.

^c Qianwan Institute of CNITECH, Ningbo 315336, China.

^d University of Chinese Academy of Sciences, Beijing 100049, China.

^e Department of Chemistry and Biochemistry, University of Notre Dame, Notre Dame, IN 46556, USA.

^f School of Energy and Power Engineering, Xi'an Jiaotong University, Xi'an 710049, China.

* Corresponding author: zhangleiucd@nimte.ac.cn.

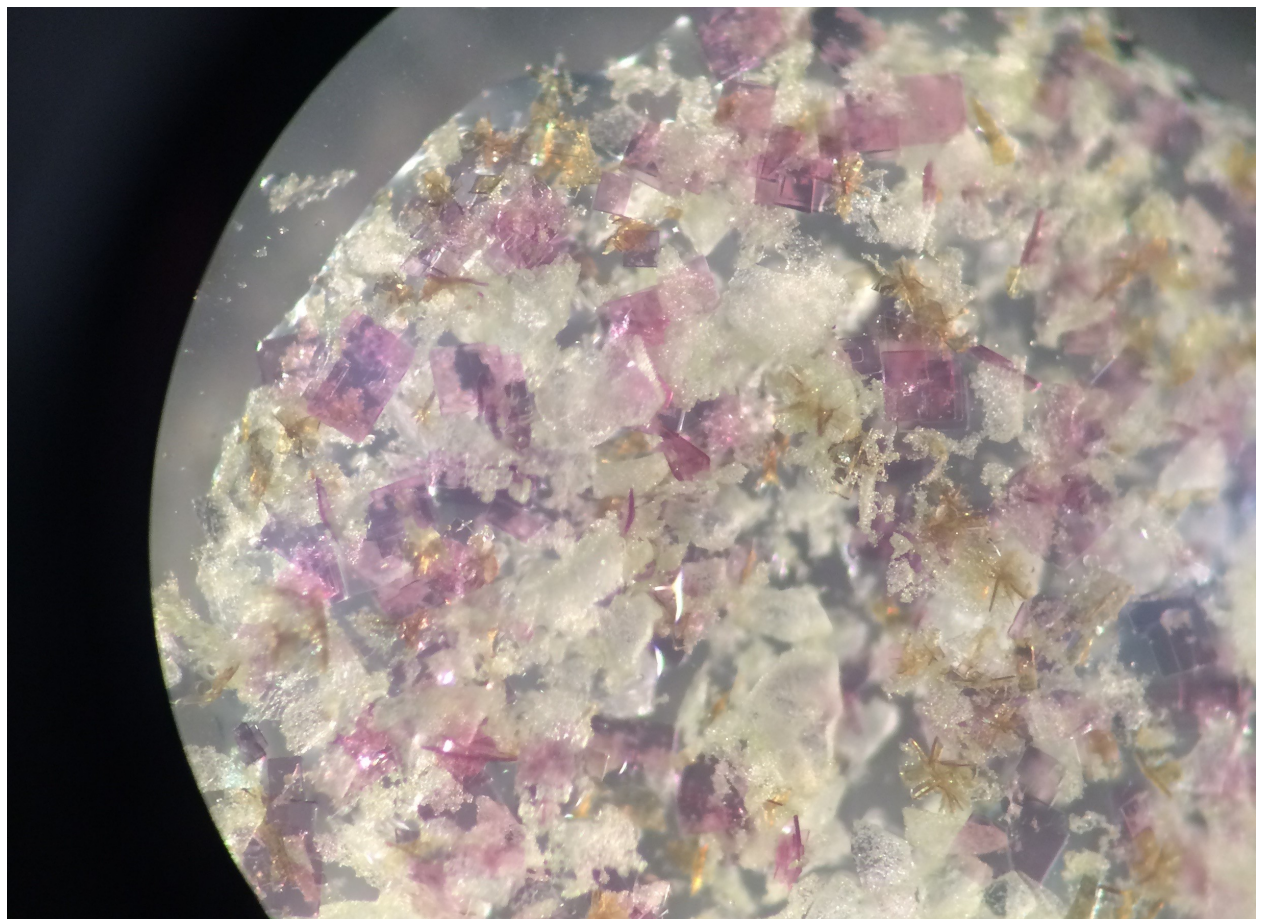


Fig. S1. Brown plate crystal agglomerates of $(\text{NpO}_2)_3(\text{PO}_4)_2(\text{Terpy})$, and pink square crystals of $\text{K}[(\text{NpO}_2)(\text{PO}_4)](\text{H}_2\text{O})_3$, formed from the hydrothermal reactions.

Table S1. Crystallographic data and details of the structure refinement for $(\text{NpO}_2)_3(\text{PO}_4)_2(\text{Terpy})$.

Chemical formula	$\text{C}_{15}\text{H}_{11}\text{N}_3\text{Np}_3\text{O}_{14}\text{P}_2$
Formula weight	1230.36
Temperature/K	298
Crystal system	Orthorhombic
Space group	$\text{Pca}2_1$
a/Å	13.9944(8)
b/Å	12.1989(7)
c/Å	13.1277(8)
$\alpha/^\circ$	$\alpha = \beta = \gamma = 90$
Volume/Å ³	2241.1(2)
Z	4
$\rho_{\text{calc}}/\text{g/cm}^3$	3.647
μ/mm^{-1}	14.031
F(000)	543.0
Crystal size/mm ³	0.020×0.020×0.002
Radiation	MoKα ($\lambda = 0.71073$)
Index ranges	-18 ≤ h ≤ 18, -15 ≤ k ≤ 15, -17 ≤ l ≤ 17
Reflections collected	25503
Independent reflections	5463 [$R_{\text{int}} = 0.0302$, $R_{\text{sigma}} = 0.0236$]
Data/restraints/parameters	5463/1/299
Goodness-of-fit on F^2	1.070
Final R indexes [I>=2σ (I)]	$R_1 = 0.0176$, $wR_2 = 0.0453$
Final R indexes [all data]	$R_1 = 0.0180$, $wR_2 = 0.0456$
Largest diff. peak/hole / e Å ⁻³	2.03/-1.29
Flack parameter	0.365(18)

Table S2. Atomic parameters and displacement parameters for $(\text{NpO}_2)_3(\text{PO}_4)_2(\text{Terpy})$.

Atom	x	y	z	U(eq)
Np1	15122.1(2)	262.4(3)	4817.4(2)	11.16(6)
Np2	12616.6(2)	11.3(2)	3351.7(2)	10.79(7)
Np3	16162.4(2)	3119.5(2)	1533.5(3)	16.88(7)
P1	15096.1(12)	579.2(19)	2423.6(14)	10.7(4)
P2	12676.5(12)	-496.3(15)	5708.0(13)	11.0(3)
O1	13456(4)	7(4)	5006(5)	16.6(11)
O8	12505(4)	230(4)	1638(5)	17.7(12)
O2	15005(4)	240(5)	6559(5)	18.5(13)
O3	14246(3)	482(4)	3169(4)	16.2(10)
O4	14997(4)	1691(5)	4887(5)	22.6(12)
O5	10946(3)	-311(5)	3131(4)	16.0(11)
O6	16799(3)	500(4)	4988(4)	15.7(10)
O9	12331(4)	1396(4)	3535(4)	22.4(12)
O7	15266(4)	-1159(5)	4738(5)	24.5(12)
O10	12942(4)	-1363(4)	3189(4)	22.0(12)
O11	15180(4)	1738(5)	2017(4)	20.8(12)
O12	17060(4)	1651(5)	1013(4)	22.2(12)
O13	15625(5)	3211(5)	321(5)	28.6(13)
O15	16702(4)	3144(5)	2735(5)	28.2(14)
N1	14721(3)	4061(4)	2434(4)	25.1(15)
C1	14658(4)	5197(4)	2486(5)	23.3(17)
C2	13875(4)	5687(3)	2950(5)	32(2)
C3	13154(4)	5042(5)	3363(5)	36(2)
C4	13216(4)	3906(4)	3311(5)	36(2)
C5	13999(4)	3415(3)	2847(5)	34(2)
N2	16165(4)	5251(3)	1599(5)	23.0(14)
C6	16919(3)	5831(4)	1170(4)	24.0(17)
C7	16935(4)	6969(4)	1223(5)	32(2)
C8	16196(4)	7527(3)	1706(5)	35(2)
C9	15442(4)	6947(4)	2135(5)	35(2)
C10	15426(3)	5809(4)	2082(5)	26.6(18)
N3	17600(3)	4093(4)	743(5)	25.7(15)
C11	18311(4)	3457(3)	298(5)	32(2)
C12	19087(3)	3957(4)	-170(5)	33.5(19)
C13	19154(4)	5093(4)	-193(5)	34(2)
C14	18444(4)	5730(3)	252(5)	32(2)
C15	17667(4)	5230(4)	720(5)	28(2)

Table S3. Selected interatomic distances and angles in $(\text{NpO}_2)_3(\text{PO}_4)_2(\text{Terpy})$.

	Length/ Å		Angle/°		Angle/°		Angle/°
Np1-O7	1.749(5)	O7-Np1-O4	179.0(3)	O9-Np2-O6 ²	91.0(2)	O12 ⁴ -P2- O6 ²	110.6(3)
Np1-O4	1.753(6)	O7-Np1-O2	93.2(3)	O8-Np2-O6 ²	147.65(18)	O8 ⁵ -P2-O6 ²	110.9(3)
Np1-O2	2.292(7)	O4-Np1-O2	87.3(3)	O3-Np2-O6 ²	125.89(17)	O12 ⁴ -P2-O1	110.8(3)
Np1-O1	2.365(5)	O7-Np1-O1	89.4(2)	O5-Np2-O6 ²	67.49(17)	O8 ⁵ -P2-O1	111.1(3)
Np1-O6	2.376(4)	O4-Np1-O1	91.5(2)	O1-Np2-O6 ²	57.59(16)	O6 ² -P2-O1	101.3(3)
Np1-O5 ¹	2.497(5)	O2-Np1-O1	79.8(2)	O10-Np2-P2	85.67(19)	O12 ⁴ -P2- Np2	116.7(2)
Np1-O3	2.501(5)	O7-Np1-O6	90.7(2)	O9-Np2-P2	93.47(19)	O8 ⁵ -P2-Np2	131.6(2)
Np1-P1	3.1664(1 9)	O4-Np1-O6	88.4(2)	O8-Np2-P2	174.84(14)	O6 ² -P2-Np2	51.80(19)
Np1- Np2 ¹	4.0001(4)	O2-Np1-O6	88.74(18)	O3-Np2-P2	96.98(13)	O1-P2-Np2	50.2(2)
Np1- Np2	4.0113(4)	O1-Np1-O6	168.6(2)	O5-Np2-P2	96.46(14)	P2-O1-Np1	143.7(3)
Np2- O10	1.751(5)	O7-Np1-O5 ¹	85.3(2)	O1-Np2-P2	28.94(12)	P2-O1-Np2	100.8(2)
Np2-O9	1.753(5)	O4-Np1-O5 ¹	93.9(2)	O6 ² -Np2-P2	28.98(11)	Np1-O1- Np2	112.1(2)
Np2-O8	2.270(6)	O2-Np1-O5 ¹	156.57(17)	O10-Np2- Np1 ²	101.85(18)	P2 ⁶ -O8-Np2	137.2(3)
Np2-O3	2.364(5)	O1-Np1-O5 ¹	123.5(2)	O9-Np2- Np1 ²	79.35(18)	P1 ⁴ -O2-Np1	139.5(4)
Np2-O5	2.388(5)	O6-Np1-O5 ¹	67.93(17)	O8-Np2- Np1 ²	115.22(14)	P1-O3-Np2	145.7(3)
Np2-O1	2.469(6)	O7-Np1-O3	96.4(2)	O3-Np2- Np1 ²	155.65(12)	P1-O3-Np1	100.3(2)
Np2-O6 ²	2.513(5)	O4-Np1-O3	83.7(2)	O5-Np2- Np1 ²	35.93(13)	Np2-O3- Np1	111.04(1 9)
Np2-P2	3.1558(1 8)	O2-Np1-O3	146.01(17)	O1-Np2- Np1 ²	89.54(12)	P1 ² -O5-Np2	149.5(3)
Np2- Np1 ²	4.0001(4)	O1-Np1-O3	67.77(18)	O6 ² -Np2- Np1 ²	33.97(10)	P1 ² -O5- Np1 ²	100.5(2)
Np3- O15	1.749(6)	O6-Np1-O3	123.55(17)	P2-Np2-Np1 ²	62.31(3)	Np2-O5- Np1 ²	109.9(2)
Np3- O13	1.764(6)	O5 ¹ -Np1-O3	57.10(16)	O10-Np2- Np1	84.52(17)	P2 ¹ -O6-Np1	147.1(3)
Np3- O11	2.265(6)	O7-Np1-P1	93.6(2)	O9-Np2-Np1	93.43(18)	P2 ¹ -O6- Np2 ¹	99.2(2)
Np3- O12	2.292(5)	O4-Np1-P1	85.9(2)	O8-Np2-Np1	121.78(14)	Np1-O6- Np2 ¹	109.80(1 8)
Np3-N3	2.557(4)	O2-Np1-P1	172.10(15)	O3-Np2-Np1	35.59(12)	P1-O11- Np3	147.1(4)
Np3-N2	2.602(3)	O1-Np1-P1	96.24(15)	O5-Np2-Np1	157.87(13)	P2 ³ -O12- Np3	160.4(4)
Np3-N1	2.605(4)	O6-Np1-P1	95.17(13)	O1-Np2-Np1	33.11(12)	C1-N1-C5	120
P1-O11	1.516(6)	O5 ¹ -Np1-P1	28.66(11)	O6 ² -Np2- Np1	90.38(10)	C1-N1-Np3	120.7(2)

P1-O2 ³	1.519(6)	O3-Np1-P1	28.68(11)	P2-Np2-Np1	61.42(3)	C5-N1-Np3	119.3(2)
P1-O5 ¹	1.544(5)	O7-Np1-Np2 ¹	77.76(19)	Np1 ² -Np2-Np1	122.580(11)	N1-C1-C2	120
P1-O3	1.545(5)	O4-Np1-Np2 ¹	101.24(18)	O15-Np3-O13	175.4(2)	N1-C1-C10	117.5(4)
P2-O12 ⁴	1.511(6)	O2-Np1-Np2 ¹	122.76(14)	O15-Np3-O11	91.2(3)	C2-C1-C10	122.5(4)
P2-O8 ⁵	1.530(6)	O1-Np1-Np2 ¹	154.12(14)	O13-Np3-O11	92.3(3)	C3-C2-C1	120
P2-O6 ²	1.549(5)	O6-Np1-Np2 ¹	36.23(12)	O15-Np3-O12	92.6(2)	C2-C3-C4	120
P2-O1	1.555(5)	O5 ¹ -Np1-Np2 ¹	34.14(11)	O13-Np3-O12	90.8(2)	C5-C4-C3	120
O8-P2 ⁶	1.530(6)	O3-Np1-Np2 ¹	91.17(11)	O11-Np3-O12	80.5(2)	C4-C5-N1	120
O2-P1 ⁴	1.519(6)	P1-Np1-Np2 ¹	62.79(3)	O15-Np3-N3	91.1(3)	C6-N2-C10	120
O5-P1 ²	1.544(5)	O7-Np1-Np2	89.8(2)	O13-Np3-N3	86.6(3)	C6-N2-Np3	119.8(3)
O5-Np1 ²	2.497(5)	O4-Np1-Np2	90.78(18)	O11-Np3-N3	159.52(18)	C10-N2-Np3	120.2(3)
O6-P2 ¹	1.549(5)	O2-Np1-Np2	114.52(14)	O12-Np3-N3	79.09(18)	N2-C6-C7	120
O6-Np2 ¹	2.513(5)	O1-Np1-Np2	34.77(14)	O15-Np3-N2	87.3(2)	N2-C6-C15	118.0(4)
O12-P2 ³	1.511(6)	O6-Np1-Np2	156.67(12)	O13-Np3-N2	88.1(2)	C7-C6-C15	122.0(4)
N1-C1	1.39	O5 ¹ -Np1-Np2	88.87(11)	O11-Np3-N2	137.31(19)	C8-C7-C6	120
N1-C5	1.39	O3-Np1-Np2	33.37(11)	O12-Np3-N2	142.21(18)	C7-C8-C9	120
C1-C2	1.39	P1-Np1-Np2	61.52(3)	N3-Np3-N2	63.14(16)	C8-C9-C10	120
C1-C10	1.412(5)	Np2 ¹ -Np1-Np2	121.717(10)	O15-Np3-N1	85.3(2)	C9-C10-N2	120
C2-C3	1.39	O10-Np2-O9	177.9(3)	O13-Np3-N1	92.9(2)	C9-C10-C1	121.4(4)
C3-C4	1.39	O10-Np2-O8	90.6(2)	O11-Np3-N1	74.38(19)	N2-C10-C1	118.5(4)
C4-C5	1.39	O9-Np2-O8	90.4(2)	O12-Np3-N1	154.72(18)	C11-N3-C15	120
N2-C6	1.39	O10-Np2-O3	88.3(2)	N3-Np3-N1	126.09(14)	C11-N3-Np3	118.3(2)
N2-C10	1.39	O9-Np2-O3	90.0(2)	N2-Np3-N1	62.97(16)	C15-N3-Np3	121.7(2)
C6-C7	1.39	O8-Np2-O3	86.42(18)	O11-P1-O2 ³	110.9(3)	C12-C11-N3	120
C6-C15	1.408(5)	O10-Np2-O5	94.7(2)	O11-P1-O5 ¹	110.5(3)	C11-C12-C13	120
C7-C8	1.39	O9-Np2-O5	87.3(2)	O2 ³ -P1-O5 ¹	112.5(3)	C14-C13-C12	120
C8-C9	1.39	O8-Np2-O5	80.31(19)	O11-P1-O3	110.8(3)	C13-C14-C15	120
C9-C10	1.39	O3-Np2-O5	166.42(19)	O2 ³ -P1-O3	110.6(3)	C14-C15-N3	120
N3-C11	1.39	O10-Np2-O1	88.9(2)	O5 ¹ -P1-O3	101.3(3)	C14-C15-C6	122.6(4)
N3-C15	1.39	O9-Np2-O1	89.4(2)	O11-P1-Np1	117.6(2)	N3-C15-C6	117.4(4)

C11-C12	1.39	O8-Np2-O1	154.75(18)	O2 ³ -P1-Np1	131.5(3)		
C12-C13	1.39	O3-Np2-O1	68.33(17)	O5 ¹ -P1-Np1	50.8(2)		
C13-C14	1.39	O5-Np2-O1	124.89(19)	O3-P1-Np1	51.00(19)		
C14-C15	1.39	O10-Np2-O6 ²	89.1(2)	O12 ⁴ -P2-O8 ⁵	111.6(3)		

Symmetry codes: ¹1/2+X,-Y,+Z; ²-1/2+X,-Y,+Z; ³3-X,-Y,-1/2+Z; ⁴3-X,-Y,1/2+Z; ⁵5/2-X,+Y,1/2+Z; ⁶5/2-X,+Y,-1/2+Z

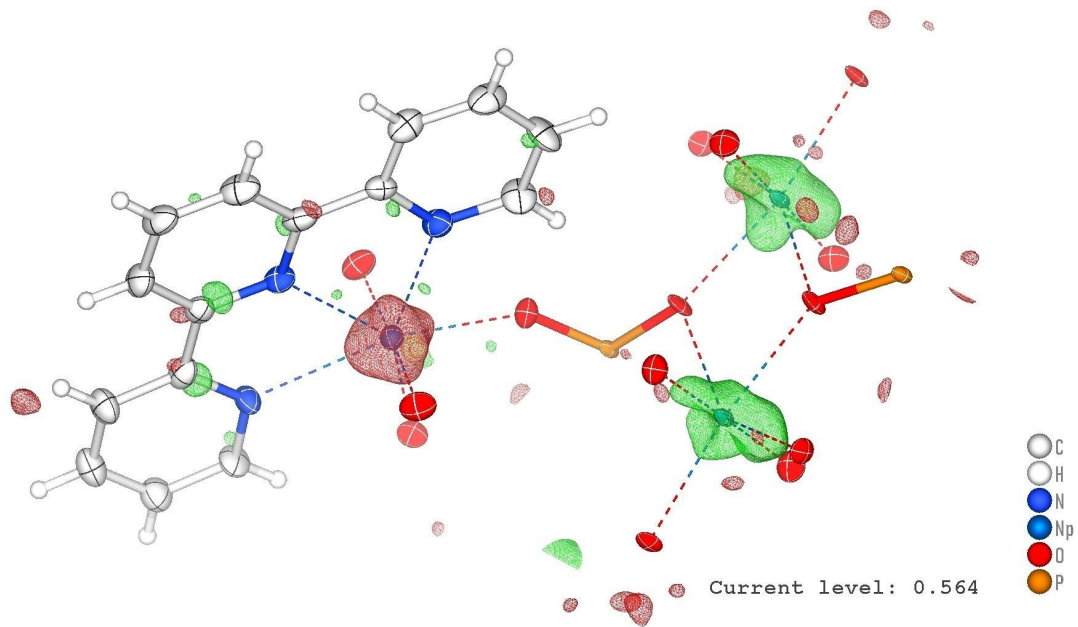


Fig. S2. Residual density plot of $(\text{NpO}_2)_3(\text{PO}_4)_2(\text{Terpy})$.

When refining the occupancies of Np freely, Np1 and Np2 refine to an occupancy of 1, while Np3 refines to an occupancy of 95%. This may be the result of a lower electron density surrounding of Np3, which is bonded to terpyridine ($\text{C}_{15}\text{H}_{11}\text{N}_3$) and two PO_4 tetrahedra. Unlike Np1 and Np2, they form a $(\text{NpO}_2)_2(\text{PO}_4)_2^{2-}$ chain by edge-sharing.

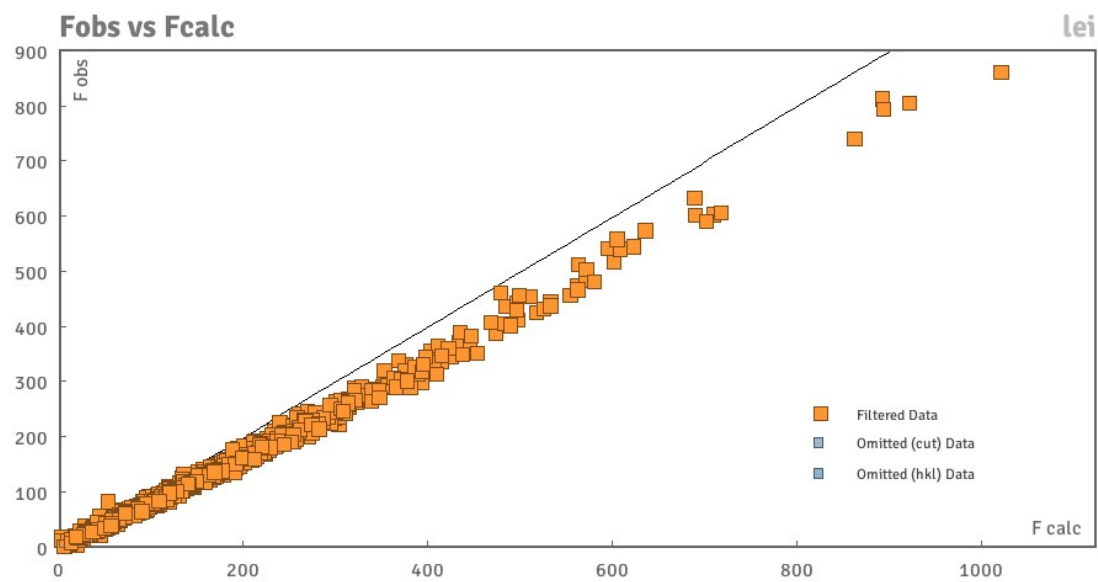


Fig. S3. Fobs vs Fcalc plot of $(\text{NpO}_2)_3(\text{PO}_4)_2$ (Terpy).

All reflections are slightly weaker than expected, but none of them has a $| \text{Error/esd} |$ value larger than 10. This might be the result of a systematic deviation of the F factors involving Np, which we don't have a sound explanation for the observed.

Table S4. Bond valence calculations of Np in $(\text{NpO}_2)_3(\text{PO}_4)_2(\text{Terpy})$.

	Np(1)	Np(2)	Np(3)
O(1)	1.7487	1.7503	1.7490
O(2)	1.7539	1.7524	1.7640
O(3)	2.2923	2.2708	2.2656
O(4)	2.3653	2.3636	2.2921
O(5)	2.3751	2.3884	
O(6)	2.4968	2.4691	
O(7)	2.5015	2.5125	
N(1)			2.5563
N(2)			2.6016
N(3)			2.6049
Σ	5.783	5.811	5.722

Note: Bond valence calculation for Np in $(\text{NpO}_2)_3(\text{PO}_4)_2(\text{Terpy})$ using bond valences parameters $R_{ij} = 2.022 \text{ \AA}$ and $b = 0.523 \text{ \AA}$ for Np-O¹. The parameters related to Np-N were not investigated, so the bond valences parameters $R_{ij} = 2.24 \text{ \AA}$ and $b = 0.37 \text{ \AA}$ of the similar U-N were used instead².

Crystal structure of $(\text{NpO}_2)_3(\text{PO}_4)_2(\text{Terpy})$

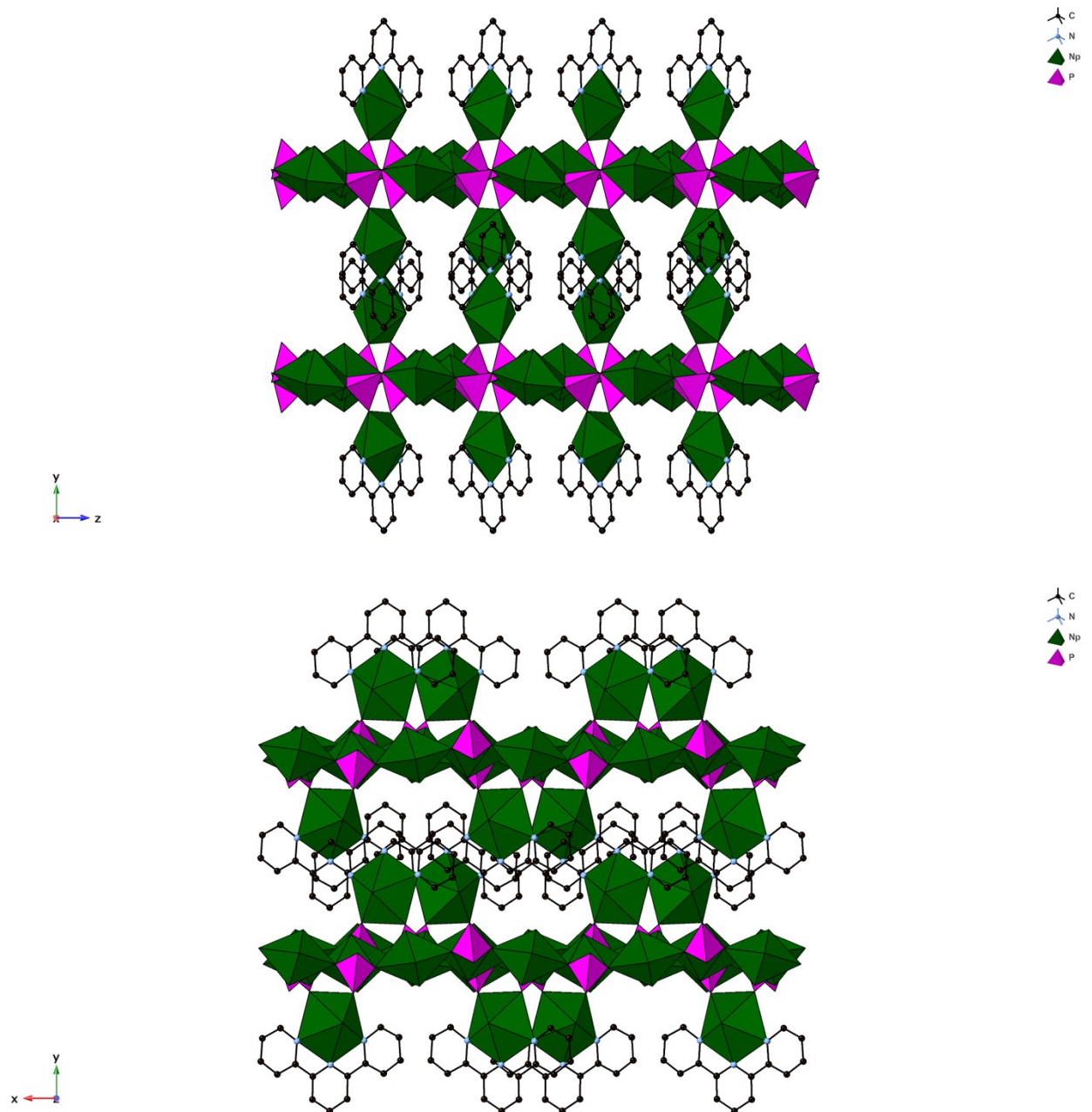


Fig. S4. Crystal structure of $(\text{NpO}_2)_3(\text{PO}_4)_2(\text{Terpy})$ as viewed down (a) the crystallographic a axis, and (b) the crystallographic c axis.

Powder X-ray Diffraction (PXRD)

The $(\text{UO}_2)_3(\text{PO}_4)_2(\text{Terpy})$ powders were washed with de-ionized H_2O , dried, and ground. The dried powers were then characterized by powder X-ray diffraction using a D8 ADVANCE X-ray diffractometer with a Cu $\text{K}\alpha$ source ($\lambda = 1.54056 \text{ \AA}$) and a Lynxeye detector.

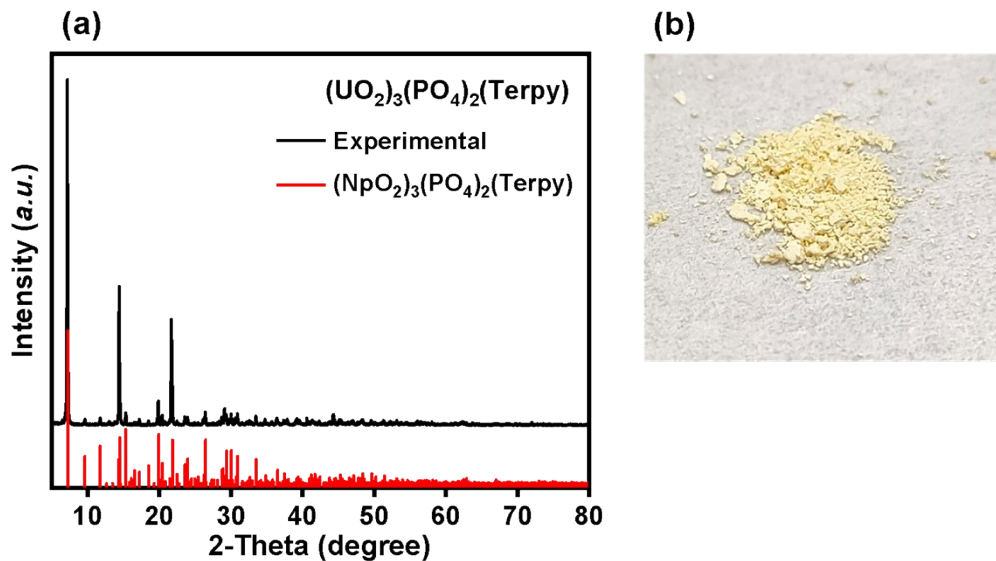


Fig. S5. (a) Experimental (black) powder diffraction pattern of $(\text{UO}_2)_3(\text{PO}_4)_2(\text{Terpy})$, and the theoretical diffraction pattern (red) calculated using Crystalmaker software from $(\text{NpO}_2)_3(\text{PO}_4)_2(\text{Terpy})$ single crystal structure; (b) Optical images of $(\text{UO}_2)_3(\text{PO}_4)_2(\text{Terpy})$ powder sample.

Energy-Dispersive Spectroscopy (EDS)

The elements in the $(\text{UO}_2)_3(\text{PO}_4)_2(\text{Terpy})$ powder sample was analyzed using data collected on a ZEISS GeminiSEM 300 equipped with an EDS detector. SEM imaging shows a scaly structure on the surface of the powder sample. EDS verified the presence of U, P, N, O (except for H which cannot be detected by the instrument).

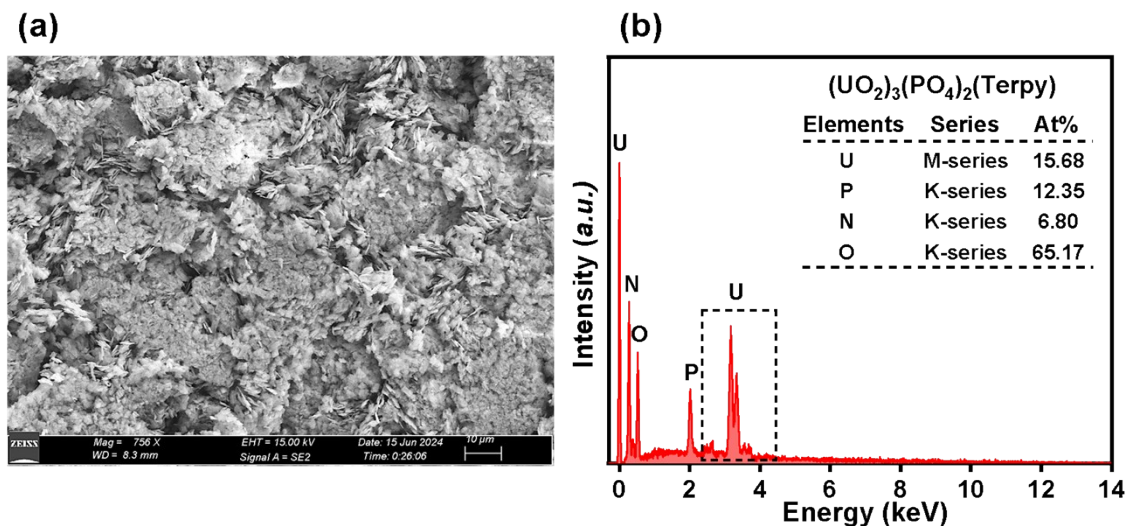


Fig. S6. SEM image of powder sample of $(\text{UO}_2)_3(\text{PO}_4)_2(\text{Terpy})$ (a) and EDS analysis results (b).

Table S5. The semi-quant results of $(\text{UO}_2)_3(\text{PO}_4)_2(\text{Terpy})$ powder by EDS analysis. For convenience of comparison, all elemental ratios are divided by U=1.

At%	U	P	N	O
$(\text{UO}_2)_3(\text{PO}_4)_2(\text{Terpy})$	1.00	0.79	0.43	4.16

Fourier Transform Infrared (FTIR) spectroscopy

FTIR spectrum of $(\text{UO}_2)_3(\text{PO}_4)_2(\text{Terpy})$ samples were measured at room temperature using Nicolet iS20 FTIR spectrometer (compaction of samples in tablets with KBr), over the ranges of $450 - 2000 \text{ cm}^{-1}$ (resolution 4 cm^{-1} , 32 scans).

In FTIR spectrum of uranyl ion within the range of $700 - 1000 \text{ cm}^{-1}$ is shown in Figure S5, the typical stretching vibration of $(\text{UO}_2)^{2+}$ units can be observed at $\sim 930 \text{ cm}^{-1}$ ^[3-5]. It is also known that the band at $1000 - 1170 \text{ cm}^{-1}$ is characteristic of $(\text{PO}_4)^{3-}$ ligands⁶⁻⁸.

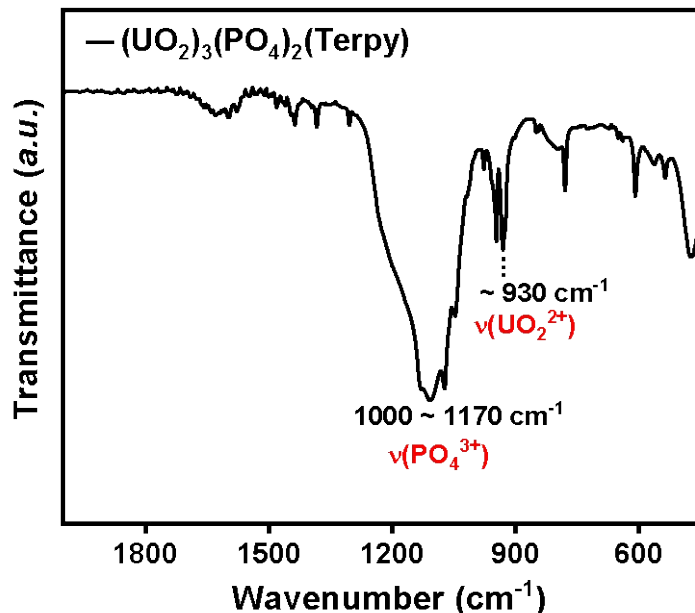


Fig. S7. FTIR spectrum for $(\text{UO}_2)_3(\text{PO}_4)_2(\text{Terpy})$ shown over $450-2000 \text{ cm}^{-1}$.

UV–Vis Diffuse Reflectance Spectroscopy

UV-Vis diffuse reflectance spectra of $(\text{UO}_2)_3(\text{PO}_4)_2(\text{Terpy})$ samples were collected by a Hitachi UH-4150 UV-Vis spectrophotometer for the range of 200 – 800 nm. The four typical bands of the uranyl group located at 403, 415, 427 and 441 nm are present in the spectrum of $(\text{UO}_2)_3(\text{PO}_4)_2(\text{Terpy})$ (vs 404, 416, 429 and 444 nm which are the peak value for the red line portion of the structure $\text{U}(\text{UO}_2)(\text{PO}_4)_2$ in Figure S6)⁹, suggesting its formula being $(\text{U}^{\text{VI}}\text{O}_2)_3(\text{PO}_4)_2(\text{Terpy})$.

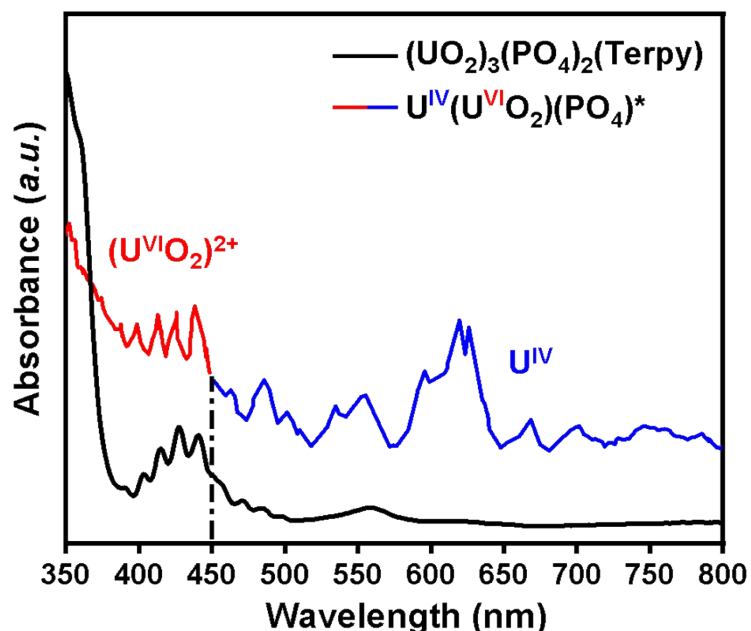


Fig. S8. UV-visible absorption spectra of $(\text{UO}_2)_3(\text{PO}_4)_2(\text{Terpy})$ (black) and $\text{U}(\text{UO}_2)(\text{PO}_4)_2$ (characteristic peaks for U^{IV} (blue) above 450 nm is the, and uranyl ions (red) below 450 nm).

Confocal Micro-Raman Spectroscopy

Raman spectroscopic studies of $(\text{UO}_2)_3(\text{PO}_4)_2(\text{Terpy})$ were carried out using a LabRAM HR Evolution instrument with an argon laser working at 532 nm output. Spectra were recorded in the range of $200 - 2000 \text{ cm}^{-1}$. A tentative assignment is provided for most of the experimental bands, whereas the non-assigned frequencies are listed in Figure S7 and Table S6. As shown in the experimental spectra, the wavenumber region involves an overlap of several vibrational modes, and these bands concern mainly: the bands at 1400 to 1600 cm^{-1} originating from the $\nu(\text{C}=\text{C})$ and $\nu(\text{C}=\text{N})$ stretching vibrations of the pyridine rings; the band at 1341 cm^{-1} belonging to the stretching vibration $\nu(\text{C}-\text{C})$ between the rings; the band at 1294 cm^{-1} also resulting from $\nu(\text{C}=\text{C})$ and $\nu(\text{C}=\text{N})$ vibrations, and combinatory vibrations of in-plane deformation vibrations $\delta(=\text{C}-\text{H})$ of the pyridine rings; bands at 1011 and 424 cm^{-1} attributed to the $(\text{PO}_4)^{3-}$ antisymmetric stretching and bending vibrations, respectively; a low intensity band observed at 798 cm^{-1} attributed to the symmetric stretching vibration of the $(\text{UO}_2)^{2+}$ units; and in particular, the band at 865 cm^{-1} probably assigned to the water libration mode^{3,6,10-14}.

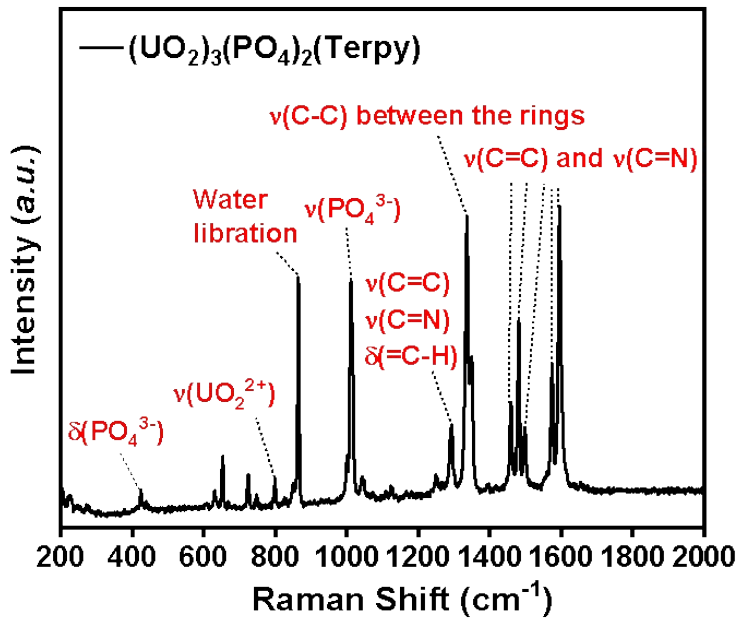


Fig. S9. Raman spectra for $(\text{UO}_2)_3(\text{PO}_4)_2(\text{Terpy})$ shown over 200-2000 cm^{-1} .

Table S6. Raman spectra assignments of $(\text{UO}_2)_3(\text{PO}_4)_2(\text{Terpy})$ powder.

Raman spectra	Band assignments
1599, 1574	$(\text{C}=\text{C})$ and $(\text{C}=\text{N})$ of the pyridine rings stretching
1498, 1480, 1458	
1341	$(\text{C}-\text{C})$ stretching between the rings
1294	Combinatory vibrations of $(\text{C}=\text{C})$ and $(\text{C}=\text{N})$ and $(=\text{C}-\text{H})$ in-plane deformation of the pyridine rings.
1011	$(\text{PO}_4)^{3-}$ antisymmetric stretching
865	Water libration
798	$(\text{UO}_2)^{2+}$ symmetric stretching
424	$(\text{PO}_4)^{3-}$ bending

Optical properties

Fluorescence data of $(\text{UO}_2)_3(\text{PO}_4)_2(\text{Terpy})$ powder were collected on a Hitachi F-4700 fluorescence spectrophotometer. The emission spectra were collected in the wavelength range of 450 – 600 nm at an excitation wavelength of 380 nm, and the results are shown in Figure S8. There are six major emission peaks between 450-600 nm at 488, 499, 507, 522, 547 and 573 nm, and the yellow powder displays the green luminescence typical of uranyl compounds under UV light^{15–19}.

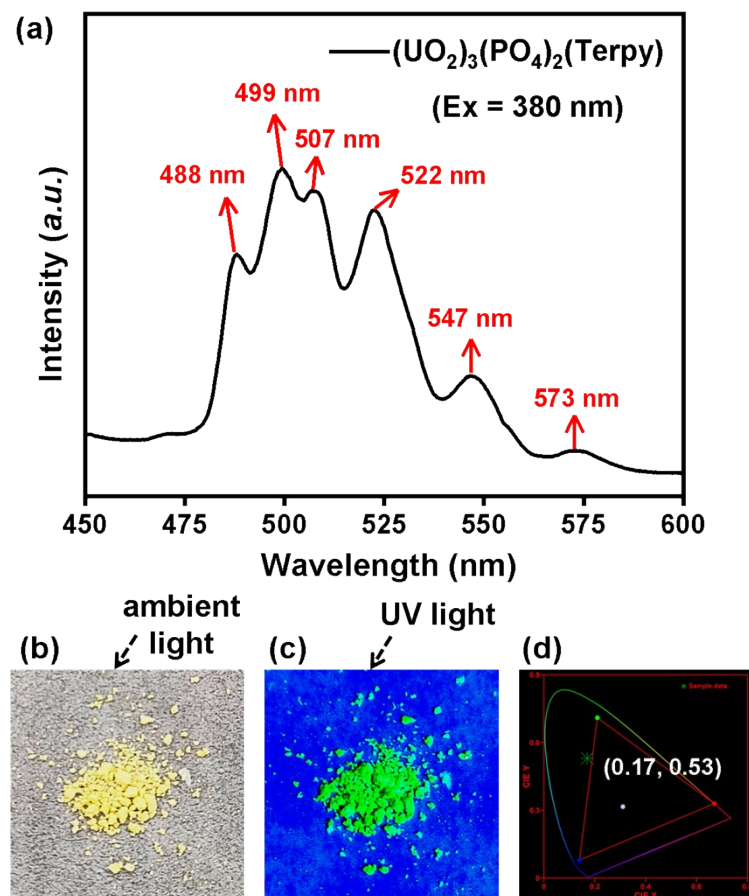


Fig. S10. (a) Fluorescence emission spectra of the $(\text{UO}_2)_3(\text{PO}_4)_2(\text{Terpy})$ powder; images of the powder under ambient light (b) and UV light (c); and (d) the CIE chromaticity diagram of $(\text{UO}_2)_3(\text{PO}_4)_2(\text{Terpy})$ with excitation at 380 nm.

REFERENCES

- (1) Gagné, O. C.; Hawthorne, F. C. Comprehensive Derivation of Bond–Valence Parameters for Ion Pairs Involving Oxygen. *Acta Crystallogr B Struct Sci Cryst Eng Mater* **2015**, *71* (Pt 5), 562–578. <https://doi.org/10.1107/S2052520615016297>.
- (2) Brese, N. E.; O’Keeffe, M. Bond–Valence Parameters for Solids. *Acta Crystallographica Section B* **1991**, *47* (2), 192–197. <https://doi.org/10.1107/S0108768190011041>.
- (3) Vitova, T.; Pidchenko, I.; Schild, D.; Prüßmann, T.; Montoya, V.; Fellhauer, D.; Gaona, X.; Bohnert, E.; Rothe, J.; Baker, R. J.; Geckeis, H. Competitive Reaction of Neptunium(V) and Uranium(VI) in Potassium–Sodium Carbonate-Rich Aqueous Media: Speciation Study with a Focus on High-Resolution X-Ray Spectroscopy. *Inorg. Chem.* **2020**, *59* (1), 8–22. <https://doi.org/10.1021/acs.inorgchem.9b02463>.
- (4) Andreev, G.; Budantseva, N.; Fedoseev, A. Crystal Structure and Spectral Properties of Np(VI) and U(VI) Methanesulfonates. *J Radioanal Nucl Chem* **2019**, *320* (2), 485–490. <https://doi.org/10.1007/s10967-019-06496-8>.
- (5) Prestianni, A.; Joubert, L.; Chagnes, A.; Cote, G.; Ohnet, M.-N.; Rabbe, C.; Charbonnel, M.-C.; Adamo, C. IR Fingerprints of U(VI) Nitrate Monoamides Complexes: A Joint Experimental and Theoretical Study. *J. Phys. Chem. A* **2010**, *114* (40), 10878–10884. <https://doi.org/10.1021/jp106467p>.
- (6) Stefanovsky, S. V.; Stefanovsky, O. I.; Kadyko, M. I. FTIR and Raman Spectroscopic Study of Sodium Aluminophosphate and Sodium Aluminum-Iron Phosphate Glasses Containing Uranium Oxides. *Journal of Non-Crystalline Solids* **2016**, *443*, 192–198. <https://doi.org/10.1016/j.jnoncrysol.2016.04.031>.
- (7) Shen, P.-P.; Wu, X.-H.; Ren, N.; Zhang, J.-J.; Wang, S.-P. Lanthanide Complexes with 2,3-Dimethoxybenzoic Acid and Terpyridine: Crystal Structures, Thermal Properties, and Antibacterial Activities. *Zeitschrift für anorganische und allgemeine Chemie*.
- (8) Corbridge, D. E. C.; Lowe, E. J. The Infra-Red Spectra of Some Inorganic Phosphorus Compounds. *J. Chem. Soc.* **1954**, No. 0, 493–502. <https://doi.org/10.1039/JR9540000493>.
- (9) Benard, P.; Louer, D.; Dacheux, N.; Brandel, V.; Genet, M. U(UO₂)(PO₄)₂, a New Mixed-Valence Uranium Orthophosphate: Ab Initio Structure Determination from Powder Diffraction Data and Optical and X-Ray Photoelectron Spectra. *Chem. Mater.* **1994**, *6* (7), 1049–1058. <https://doi.org/10.1021/cm00043a029>.
- (10) Sánchez-Pastor, N.; Pinto, A. J.; Astilleros, J. M.; Fernández-Díaz, L.; Gonçalves, M. A. Raman Spectroscopic Characterization of a Synthetic, Non-Stoichiometric Cu–Ba Uranyl Phosphate. **2013**.
- (11) Hadrich, A.; Lautie, A.; Mhiri, T. Vibrational Study and Fluorescence Bands in the FT–Raman Spectra of Ca_{10-x}Pb_x(PO₄)₆(OH)₂ Compounds. *Spectrochimica Acta Part A* **2001**, *57*, 1673–1681.
- (12) Frost, R. L.; Čejka, J.; Ayoko, G. A.; Weier, M. A Raman Spectroscopic Study of the Uranyl Phosphate Mineral Bergenite. *Spectrochimica Acta Part A: Molecular and Biomolecular Spectroscopy* **2007**, *66* (4), 979–984. <https://doi.org/10.1016/j.saa.2006.04.036>.
- (13) Lines, A. M.; Hall, G. B.; Sinkov, S.; Levitskaia, T.; Gallagher, N.; Lumetta, G. J.; Bryan, S. A. Overcoming Oxidation State-Dependent Spectral Interferences: Online Monitoring of U(VI) Reduction to U(IV) via Raman and UV–Vis Spectroscopy. *Ind. Eng. Chem. Res.* **2020**, *59* (19), 8894–8901. <https://doi.org/10.1021/acs.iecr.9b06706>.
- (14) Bonales, L. J.; Rodríguez-Villagra, N.; Sánchez-García, I.; Montoro, O. R. U(VI)

- Speciation Studies by Raman Spectroscopy Technique in the Production of Nuclear Fuel. *Progress in Nuclear Energy* **2022**, *145*, 104122. <https://doi.org/10.1016/j.pnucene.2022.104122>.
- (15) Drobot, B.; Steudtner, R.; Raff, J.; Geipel, G.; Brendler, V.; Tsushima, S. Combining Luminescence Spectroscopy, Parallel Factor Analysis and Quantum Chemistry to Reveal Metal Speciation – a Case Study of Uranyl(VI) Hydrolysis. *Chem. Sci.* **2015**, *6* (2), 964–972. <https://doi.org/10.1039/C4SC02022G>.
- (16) Wang, Z.; Zachara, J. M.; Gassman, P. L.; Liu, C.; Qafoku, O.; Yantasee, W.; Catalano, J. G. Fluorescence Spectroscopy of U(VI)-Silicates and U(VI)-Contaminated Hanford Sediment. *Geochimica et Cosmochimica Acta* **2005**, *69* (6), 1391–1403. <https://doi.org/10.1016/j.gca.2004.08.028>.
- (17) Thangavelu, S. G.; Pope, S. J. A.; Cahill, C. L. Synthetic, Structural, and Luminescence Study of Uranyl Coordination Polymers Containing Chelating Terpyridine and Trispyridyltriazine Ligands. *CrystEngComm* **2015**, *17* (32), 6236–6247. <https://doi.org/10.1039/C5CE00984G>.
- (18) Meinrath, G. Uranium(VI) Speciation by Spectroscopy. *J Radioanal Nucl Chem* **1997**, *224* (1–2), 119–126. <https://doi.org/10.1007/BF02034623>.
- (19) Morrison, G.; zur Loye, H.-C. Flux Growth of $[\text{NaK}_6\text{F}][(\text{UO}_2)_3(\text{Si}_2\text{O}_7)_2]$ and $[\text{KK}_6\text{Cl}][(\text{UO}_2)_3(\text{Si}_2\text{O}_7)_2]$: The Effect of Surface Area to Volume Ratios on Reaction Products. *Crystal Growth & Design* **2016**, *16* (3), 1294–1299. <https://doi.org/10.1021/acs.cgd.5b01408>.